Chapter 5

Dye-Sensitized Solar Cells with Graphene Electron Extraction Layer

Lung-Chien Chen

Additional information is available at the end of the chapter

http://dx.doi.org/10.5772/60644

Abstract

This work aims to improve the conversion efficiency of dye-sensitized solar cells (DSSCs) by introducing a new material, graphene, into the DSSC structure. Graphene is a potential material for many applications due to their high electron mobility, outstanding optical properties, and thermal, chemical, and mechanical stability. Therefore, this study changes several parameters, structures, and methods to optimize and compare with the traditional DSSCs. There are three major respects about with or without graphene, the method of plating or sputtering, and the structure of graphene/TiO_2 or TiO_2/graphene/TiO_2 in DSSCs solar cells. Finally, this research knows that the method of sputtering is much better than plating; the conversion efficiency of solar energy with graphene/TiO_2 was increased from 1.45 % to 3.98 %, and the conversion efficiency with TiO_2/graphene/TiO_2 sandwich structure was increased from 1.38 % to 3.93 %. It means that the new material, graphene, works in enhancing the conversion efficiency of DSSCs.

Keywords: DSSCs, Solar cell, Graphene, Sandwich structure, TiO_2

1. Introduction

This chapter aims to review the dye-sensitized solar cells (DSSCs) with graphene structure. DSSCs have been under extensive research. Since the color of the device can be easily varied by choosing different dyes and cells on flexible substrates have been already demonstrated, DSSCs are especially attractive for building integrated photovoltaics. The cell concept can

reduce the production costs and energy payback time significantly compared to standard silicon cells or other thin film cells.

However, one of the major issues hindering the rapid commercialization of DSSCs is their lower conversion efficiency compared to conventional p-n junction solar cells [1]. That may be attributed to poor charge separation in DSSC structure. Therefore, charge transfer structure, such as Au nanoparticles and quantum dots, has been employed in a DSSC to improve the device performance through charge separation in the photoelectrodes [2-5].

Graphene is a potential material for many applications due to their high electron mobility, outstanding optical properties, and thermal, chemical, and mechanical stability [6-10]. Therefore, the second section in this article illustrates the principle of electron extraction layer. TiO_2 plays an important role on the electron-extraction layer. We will discuss the electron transmission on dye-sensitized solar cells. The effect of the electron-transporting layer of the solar cell is very important. Therefore, we show the I-V characteristics of the DSSCs. The cell performance was measured, which had different electron-extraction layer structures.

The third section discusses the preparation method of the graphene. Graphene is a potential material for many applications due to their high electron mobility, outstanding optical properties, and thermal, chemical, and mechanical stability.

In the fourth section, the graphene was introduced into the DSSC structure to improve electron conversion efficiency. This study investigates the effect on the graphene layer as electron transport layer in the DSSC structure deposited by the magnetron sputtering method; in particular, it examines the performance of the DSSCs with the graphene electron transport layer.

The fifth section reveals a new DSSC structure. The structure has provided excellent performance and higher photoelectric conversion efficiency by DSSC with the TiO_2/graphene/TiO_2 sandwich structure. This section focuses on the improvement that is associated with the increase in electron transport efficiency and the absorption of light in the visible range.

The concluding paragraphs will summarize some parameters of DSSC with or without a graphene layer which was prepared by sputtering and then discuss the DSSC's parameters and reasons which have different preparation methods of graphene layer. Finally, there are some concluding remarks.

2. Principle of electron transport layer

Figure 1 sketches the structure of the basic DSSC which can be divided into several parts. They have a basic structure that comprises two conductive substrates (one is photoelectrode and the other is counter electrode), an absorbing layer of semiconductor materials, dye molecules, and a redox electrolyte. The basic principle of operation of DSSCs includes the following: (1) the light irradiates on the DSSC and the photons will pass through the photoelectrode to the dye layer which is absorbed by the photosensitizer dye molecule. (2) The photosensitizers are

http://dx.doi.org/10.5772/60644

excited from the ground state (S) to the excited state (S*). The excited electrons are injected into the conduction band of the TiO_2 electrode. This results in the oxidation of the photosensitizer (S^+). (3) Electrons are injected from the photoexcited dye into the conductive band of the semiconductor. The electrons will pass from the electric transport layer to the external circuit. (4) The oxidized photosensitizer (S^+) accepts electrons from the I^- ion redox mediator, leading to regeneration of the ground state (S), and the I^- is oxidized to the oxidized state, I_3^-, and transports the positive charges to the counter electrode. (5) The oxidized redox mediator, I_3^-, diffuses toward the counter electrode and then it is reduced to I^- ions.

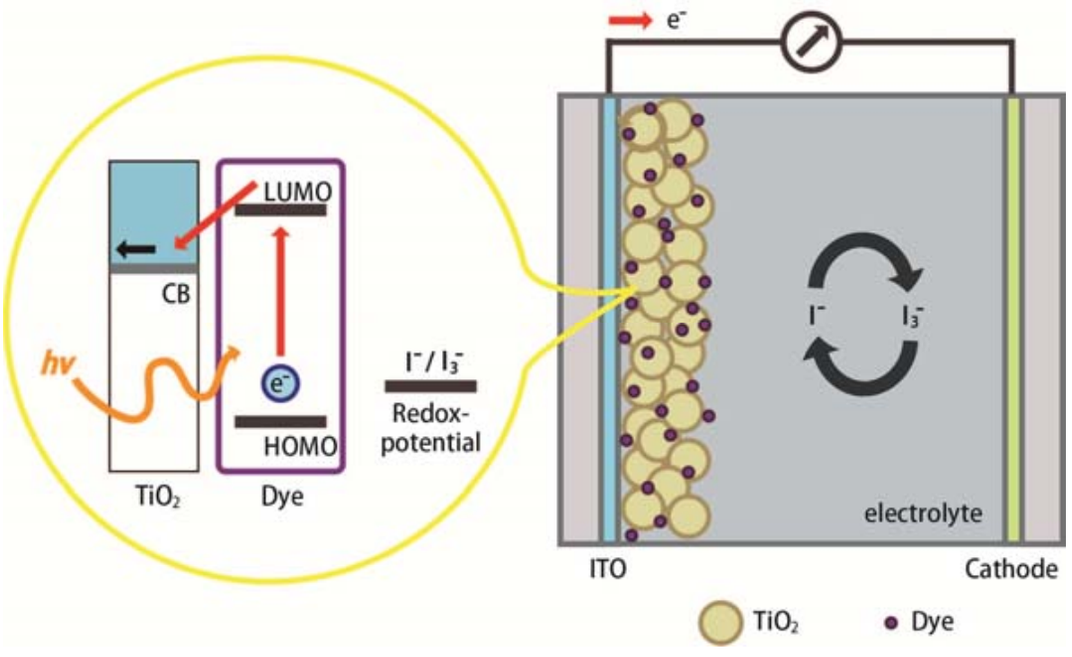

Figure 1. Schematic cross section of the completed structure

The principle of electron transport (or extraction) layer inserted in the traditional DSSC structure had been reported [11-17]. Figure 2 shows the energy level diagram and mechanism of photocurrent generation in TiO_2 DSSCs with the graphene layer. The work function of the graphene layer is around 4.5 eV [18,19]. Graphene has a work function similar to that of the indium tin oxide (ITO) (4.8 eV) electrode. The graphene layer does not prevent the flow of injected electrons down to the ITO electrode because its work function exceeds that of the ITO electrode [20-22]. Therefore, the brief operating process is as follows. Dye N719 was excited by incident light, and electrons transit from HOMO to LUMO. The LUMO and HOMO are the lowest unoccupied molecular orbit and highest occupied molecular orbit, respectively. Electrons are injected into the graphene electron transport layer via the TiO_2 photoelectrode. The electrons transferred to the graphene electron transport layer were collected at the back contact to generate a photocurrent. Therefore, the inserted graphene layer collects electrons and acts as a transporter in the effective separation of charge and rapid transport of the photogenerated electrons.

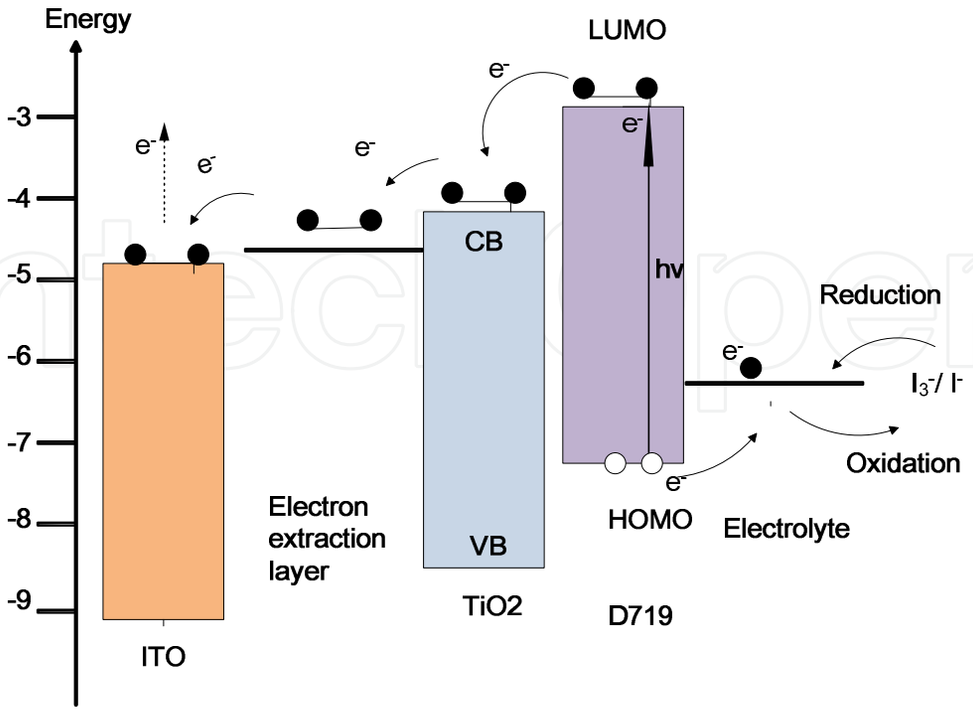

Figure 2. Energy level diagram and mechanism of photocurrent generation in the DSSCs with the graphene electron transfer layer

3. Preparation and characteristics of graphene

Graphene is a potential material for many applications such as extensively utilized in organic photovoltaic (PV) cells. It has excellent optical and electrical characteristics which are exploited in transparent conductive films or electrodes by their high electron mobility [6-8,10,17], outstanding optical properties, and thermal, chemical, and mechanical stability [6–10,12]. However, it is hard to produce high-quality graphene to use in the sputter deposition method. Therefore, this study uses plating method to plate graphene and compare with the traditional method.

First, acetylacetone and Triton X-100 were added into 10 ml water by using syringe. The TiO_2 compound solution was stirred for 24 h using a magnetic stirrer. After mixing the TiO_2 compound solution, the TiO_2 colloid is obtained. The graphene was stacked on the ITO substrate by electroplating process. The plating solution is graphene dispersion. The plating solution was injected into the beaker and stirred with an air pump. Figure 3 shows the electroplating process. The anode connected to the graphite, and the cathode connected to the ITO substrate. The speeds of the coating process were 500 rpm for 20 s and 2,000 rpm for 60 s. The thickness of TiO_2 is about 13 μm. After the annealing process by using RTA (rapid thermal annealing) at 450 °C for 30 min, the strength of the anatase structure would be enhanced. When the samples cool down to room temperature, they were soaked into the N719 solution; the

http://dx.doi.org/10.5772/60644

N719 solution is mixed ethanol and N719 powder. The samples will produce electrons when they are illuminated with light after they are soaked into the N719 solution.

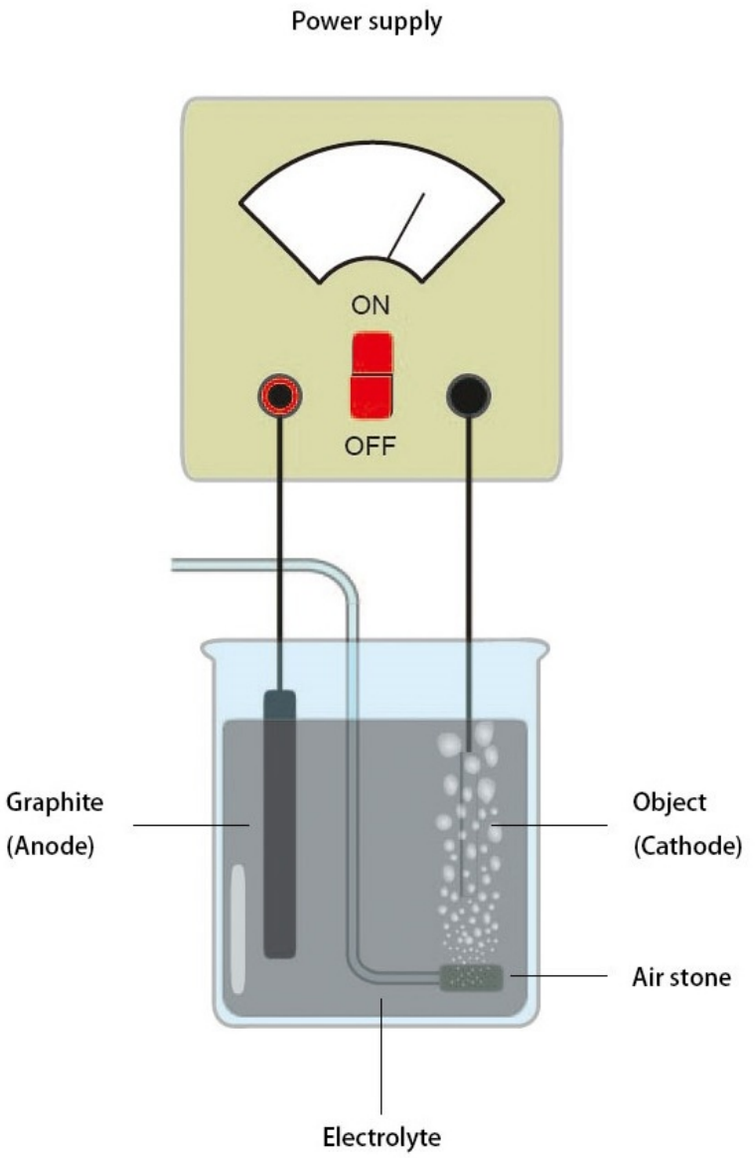

Figure 3. The graphene electroplating methods

A graphene layer was sputtered on indium tin oxide (ITO) conductive glass substrate by radio-frequency magnetron sputtering with a graphite target. It is the electron transport layer that improves the electron transfer in the DSSC structure.

First, the solution consisting of TiO_2 nanocrystalline powder, Triton X-100, acetic acid, and deionized water was mixed as a colloidal solution, and the colloidal solutions were daubed uniformly onto the graphene electron transfer layer to form a thick film. After annealing, the photoelectrode with the graphene layer was immersed in N719 dye absorption ($(Bu4N)_2$-[Ru(dcbpyH)2$(NCS)_2$] complex) in ethanol for 24 h. To increase its anatase content, the samples

were sintered at 450 for 30 min. The electrolyte was composed of iodide and lithium iodide with and without 4-tertbutylpyridine (TBP) in propylene carbonate. Then a thick layer of platinum was sputtered onto ITO substrate as a counter electrode. Cells were fabricated by placing sealing films (SX1170-60, Solaronix) between the two electrodes and leaving just two via-holes for injection of electrolyte. The sealing process was carried out on a hot plate. Then the electrolyte was injected into the space between the two electrodes through the via-holes. Finally, the via-holes were sealed using epoxy with low vapor transmission rate.

This study fabricated three different samples: samples A and B are plated with graphene for 20 min and 30 min, respectively, and sample C is a normal DSSC. Figure 4 and Table 1 show the I-V curves and the measurement values. The cell is measured under AM 1.5 illumination at 25 °C. The active area is 0.3×0.3 cm^2. The short-circuit current densities of the samples are 4.97 mA/cm^2 (electroplated with graphene for 20 min), 5.42 mA/cm^2 (electroplated with graphene for 30 min), and 11.2 mA/cm^2 (normal DSSC), respectively. The value of open-circuit voltage between the samples only has a slight difference. The efficiency of the samples are 0.796 % (electroplated with graphene for 20 min), 0.844 % (electroplated with graphene for 30 min) and 3.93 % (normal DSSC), respectively.

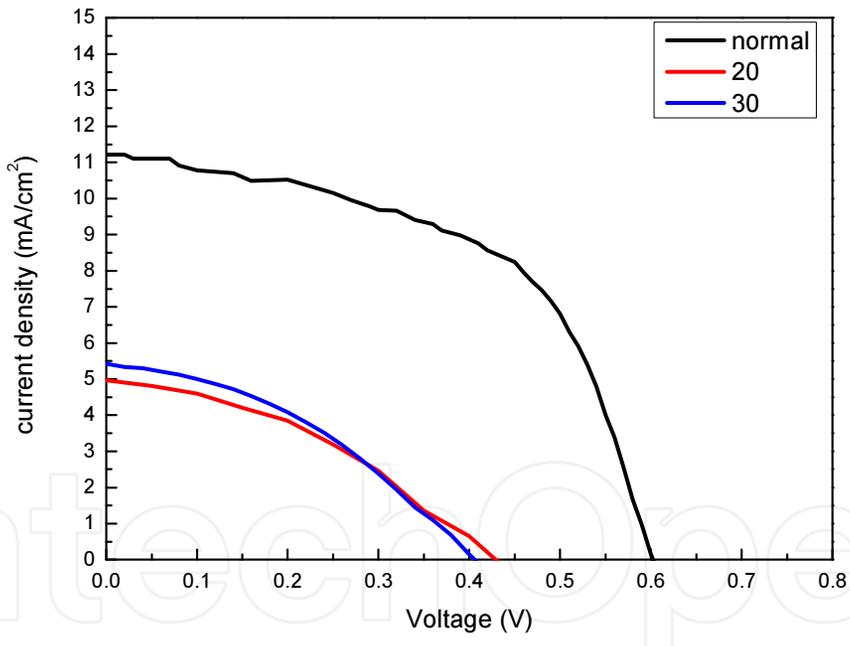

Figure 4. I-V curves of three samples

Sample	Jsc (mA/cm^2)	Voc (mV)	FF%	Efficiency (%)
A(20 min)	4.97	0.4	0.401 %	0.796 %
B(30 min)	5.42	0.4	0.389 %	0.844 %
C (normal DSSC)	11.2	0.6	0.585 %	3.93 %

Table 1. The measurement values of this study

http://dx.doi.org/10.5772/60644

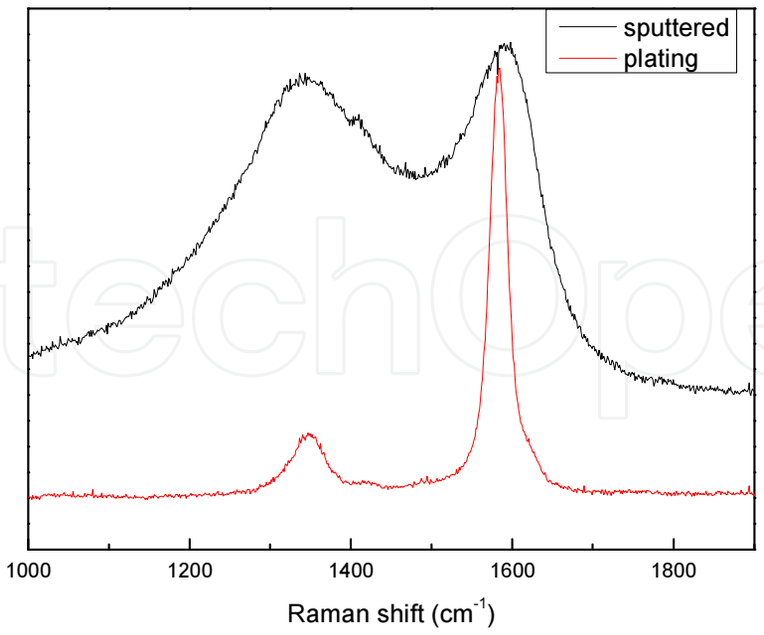

Figure 5. The Raman spectra of plated graphene and sputtered graphene in G-band and D-band

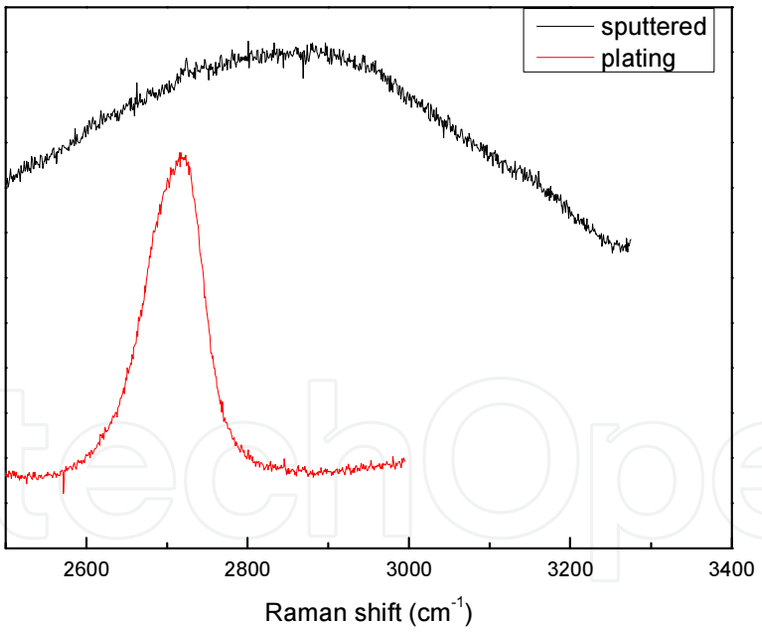

Figure 6. The Raman spectra of plated graphene and sputtered graphene in 2D-band

Figures 5 and 6 show the Raman spectra of electroplated graphene and sputtered graphene (normal DSSC). As shown in Figure 5, electroplated graphene and sputtered graphene have Raman peaks at 1,350 cm^{-1} and 1,580 cm^{-1} [23–25]. The ID/IG of plating graphene is 0.52, and the sputtered graphene is 0.96. The higher value of ID/IG shows good preservation of the highly crystalline structure of graphene. Figure 5 compares the D-band of two different

procedures [26]; it shows that using the plating process is much better than using the sputtering process. The G-band is a doubly degenerate phonon mode at the Brillouin zone center; the D-band is a defect and the phonon branches around K point [27]. As shown in Figure 6, the 2D-band is a two-phonon double-resonance process [28] and is similar to the G-band but has a more complicated peak structure [29-31]. It depends on the photon energy and polarization.

Figure 7 shows the top-view SEM image of electroplating graphene on ITO glass. As shown in Figure 7, the graphene flakes with 10 μm width were stacked on the ITO glasses. Figure 8 shows the cross-sectional SEM image of plating graphene on the ITO glass. The graphene is successfully plated on the ITO glasses, and the thickness is around 8 μm.

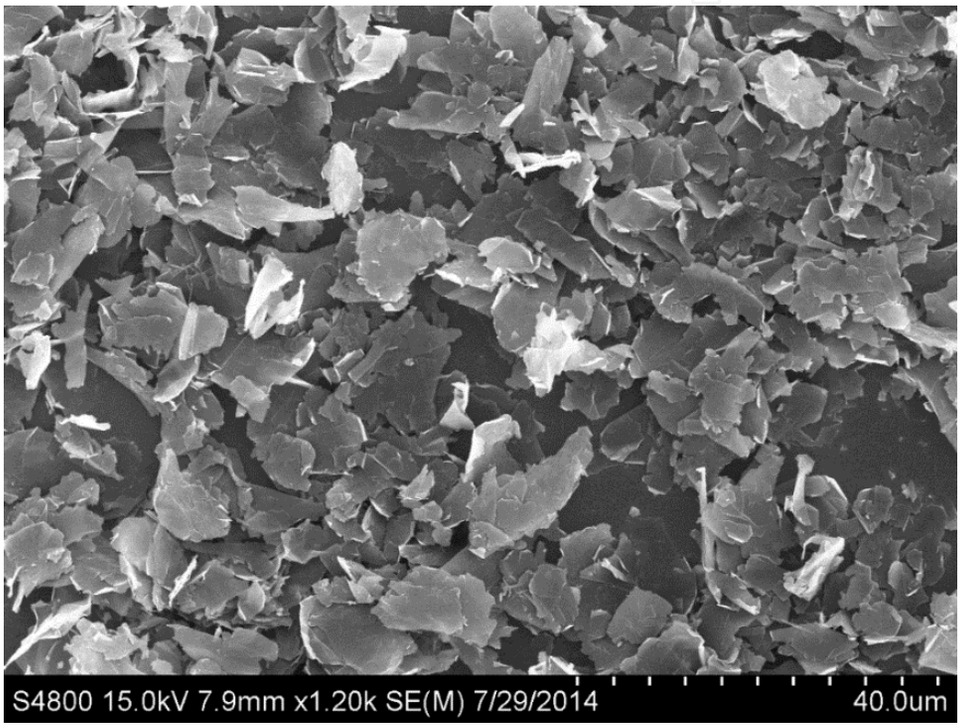

Figure 7. Top view of electroplating graphene on ITO glass surface

4. DSSCs with graphene/TiO2 active layer

Because graphene has high electron mobility, we use graphene as an electron transport layer to improve the electron transfer in the DSSC. That is DSSCs with graphene/TiO_2 active layer. The graphene flakes prepared by using the electroplating method have demonstrated a superior graphene property by Raman scattering. However, the DSSCs with graphene flakes exhibited poor power conversion efficiency, owing to the high series resistance caused by the discontinue graphene flakes. Therefore, sputtered graphene was employed to replace the graphene flakes prepared by electroplating to improve the electrical properties of the DSSCs even the sputtered graphene including graphene oxide.

http://dx.doi.org/10.5772/60644

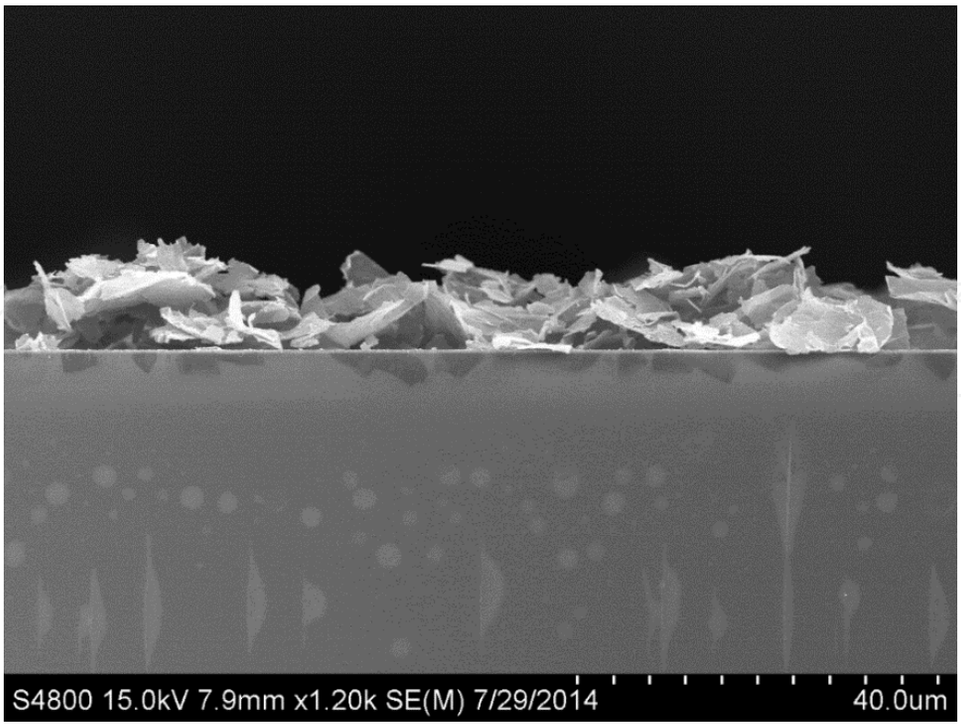

Figure 8. Cross-section SEM image of the plated graphene

First of all, a 60-nm-thick graphene layer was sputtered on indium tin oxide (ITO) conductive glass substrate by radio-frequency magnetron sputtering as an electron transport layer. Next, the solution consisting of TiO_2 was mixed as a colloidal solution which was daubed uniformly onto the graphene electron transfer layer to form a thick film. Then a 100-nm-thick layer of platinum was sputtered onto ITO substrate as a counter electrode. Cells were fabricated by placing sealing films between the two electrodes and leaving just two via-holes for injection of electrolyte. Then, the electrolyte was injected into the space between the two electrodes through the via-holes. Finally, the via-holes were sealed using epoxy with low vapor transmission rate. Figure 9 shows the cross section of the completed structure.

Afterward, we began examining its results by comparing the 60-nm-thick graphene electron transport layer with the 100-nm-thick graphene layer. Figure 10 shows the absorption of TiO_2 DSSCs with and without the graphene electron transfer layer in visible range. As shown in Figure 10, the graphene electron transport layer has an increased absorption coefficient in the range of 310–400 nm. Therefore, the graphene electron transport layer is also an absorption layer to improve the absorption of the solar cells.

Figure 11 shows the *I-V* characteristics of the DSSCs. This figure shows cell performance between TiO_2 DSSCs and TiO_2/graphene under AM 1.5 illumination with a solar intensity of 100 mW/cm^2 at 25°C. The cell has an active area of 3×3 mm^2 and no antireflective coating.

Finally, we examine its result by measuring the cell parameters, open-circuit voltage (V_{oc}), short-circuit current (J_{sc}), fill factor (FF), and energy conversion efficiency (E_{ff}) which are summarized in Table 2 [12].

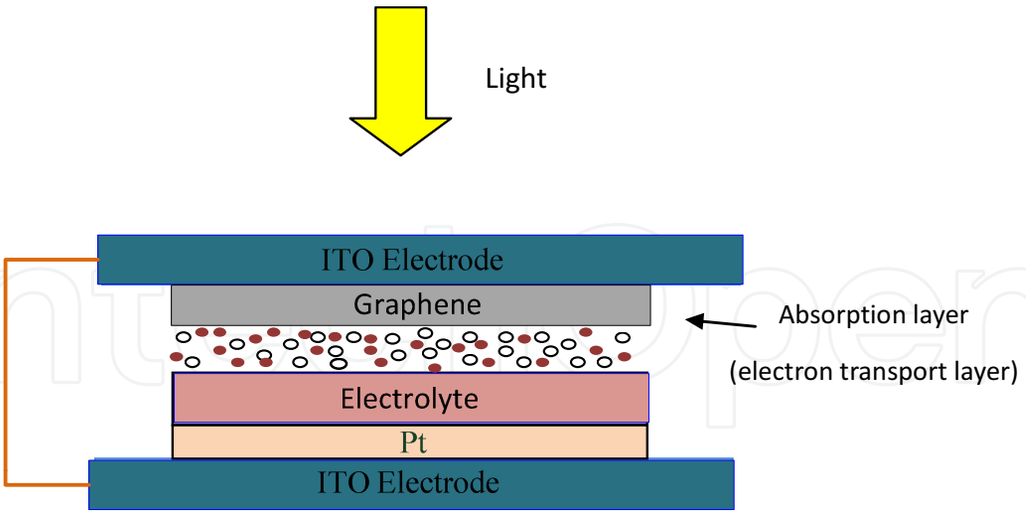

Figure 9. Schematic cross section of the completed structure

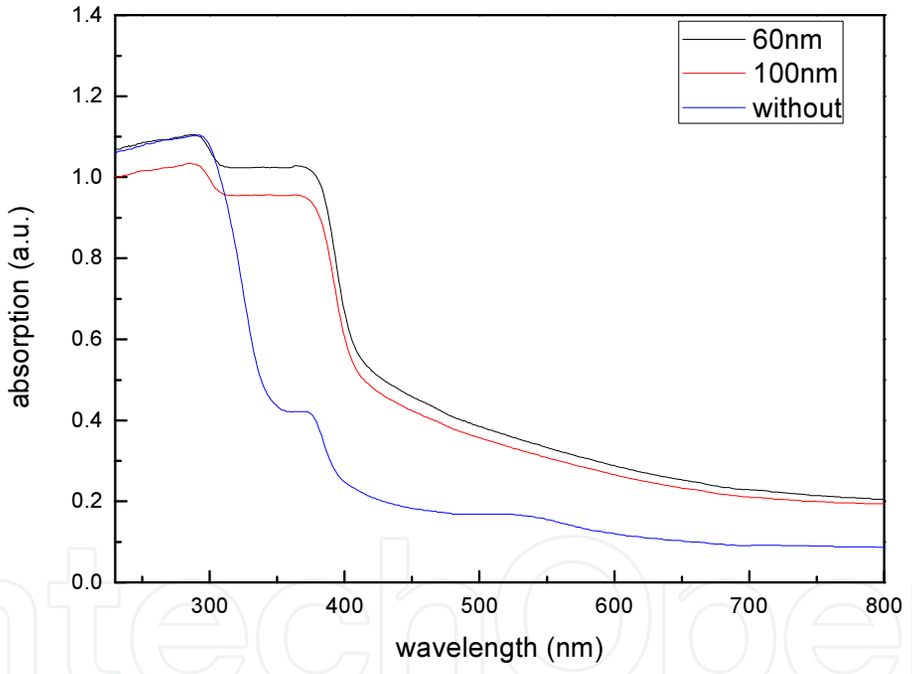

Figure 10. Absorption spectra of the DSSCs with and without the graphene electron transfer layer [12]

	TiO_2	Graphene+TiO_2
Jsc (mA/cm²)	6.9	17.5
V_{oc} (V)	0.5	0.5
FF	0.419	0.456
η (%)	1.45	3.98

Table 2. The parameters of TiO2 DSSCs with and without graphene electron transport layer [12]

http://dx.doi.org/10.5772/60644

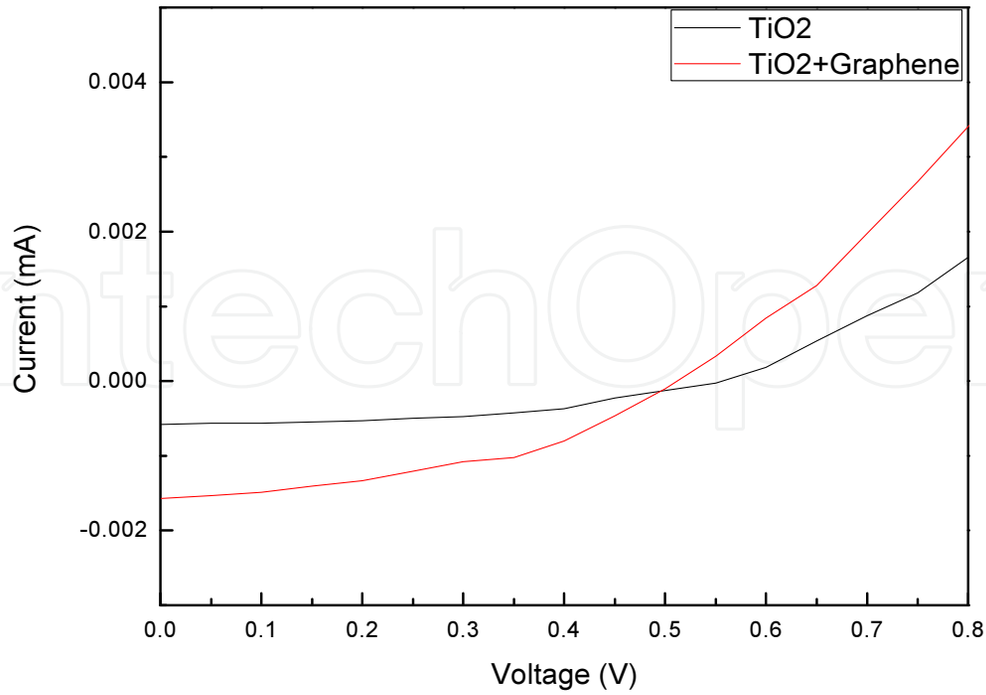

Figure 11. *I-V* curves of the DSSCs with and without the graphene electron transfer layer under illumination [12]

According to Figures 10 and 11 and Table 2, the short-circuit current rises up to 17.5, fill factor to 0.456, and energy conversion efficiency to 3.98 %. The enhanced performance of DSSCs with a graphene was attributed to the increase in electron transport efficiency and light absorption in visible range.

5. DSSCs with TiO_2/Graphene/TiO_2 sandwich structure

Because of the TiO_2/graphene sandwich structure, the efficiency on traditional DSSCs improved. As a result, we use three sandwich structures to achieve the desired outcomes of the following experiment. The enhanced performance of DSSCs with the sandwich structure can be attributed to an increase in electron transport efficiency and in the absorption of light in the visible range. The preparation of TiO_2 photoelectrodes is done by the following: the TiO_2 slurry was prepared by mixing 6 g of nanocrystalline powder, 0.1 mL Triton X-100, and 0.2 mL acetylacetone. The graphene film is deposited on the surface of the first photoelectrode layer, a single TiO_2 photoelectrode layer. This is spin-coated with the rate of rotation of 2,000 rpm, a sandwich structure with three rotational speed to 4,000 rpm, in the present experiment for comparison.

In summary, the DSSC with the sandwich structure in this study exhibited a Voc of 0.6 V, a high Jsc of 11.22 mA cm^{-2}, a fill factor (FF) of 0.58, and a calculated η of 3.93 %, which is 60 % higher than that of a DSSC with the traditional structure.

Figure 12(a) shows the top-view SEM image of the TiO_2 nanoparticles with mean diameter of 50 nm. Figure 12(b) shows the cross-sectional SEM image of a TiO_2/graphene/TiO_2 sandwich structure. The thickness of the graphene electron extraction layer is around 60 nm.

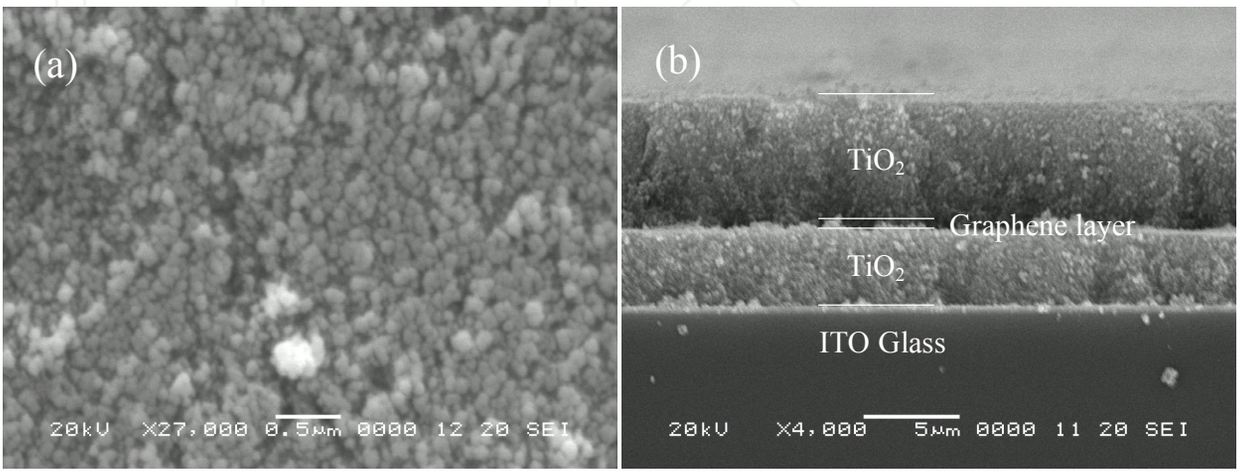

Figure 12. SEM images of (a) TiO2 nanoparticles and (b) TiO_2/graphene/TiO_2 sandwich structure [17]

Figures 13(a) and 13(b) present the Raman scattering spectra of the graphene film that was deposited on the glass substrate using the process that was described in the section on the preparation of graphene. The spectra include important peaks that correspond to the D-band (approximately 1,350 cm^{-1}), the G-band (approximately 1,580 cm^{-1}), and the 2D-band (approximately 2,700 cm^{-1}).

Figure 14 displays the UV-vis spectra of photoelectrodes with different structures before and after they were loaded with dye. Clearly, the photoelectrode with the TiO_2/graphene/TiO_2 sandwich structure has a higher absorption than those with the traditional structure both before and after loading with dye.

Figure 15 presents the energy level diagram of the DSSC with the TiO_2/graphene/TiO_2 sandwich structure. Under illumination, electrons from the photoexcited dye are transported to the conduction band (CB) of TiO_2 via the CB of the graphene and TiO_2. The transportation path via the CB of graphene is in addition to the traditional path. Owing to the excellent electrical conduction of the graphene, the graphene layer bridges behave as a channel for transferring electrons and rapidly transport the photoexcited electrons. The graphene is homogeneous throughout the system, and the excited electrons are captured by the graphene without any obstruction. The collected electrons can be rapidly and effectively transported to the CB of TiO_2 through graphene bridges. In the interface of graphene and TiO_2, the resistance through which charges are transported is reduced relative to the DSSC without graphene electron transport layer, and the recombination and back-reaction processes are suppressed.

http://dx.doi.org/10.5772/60644

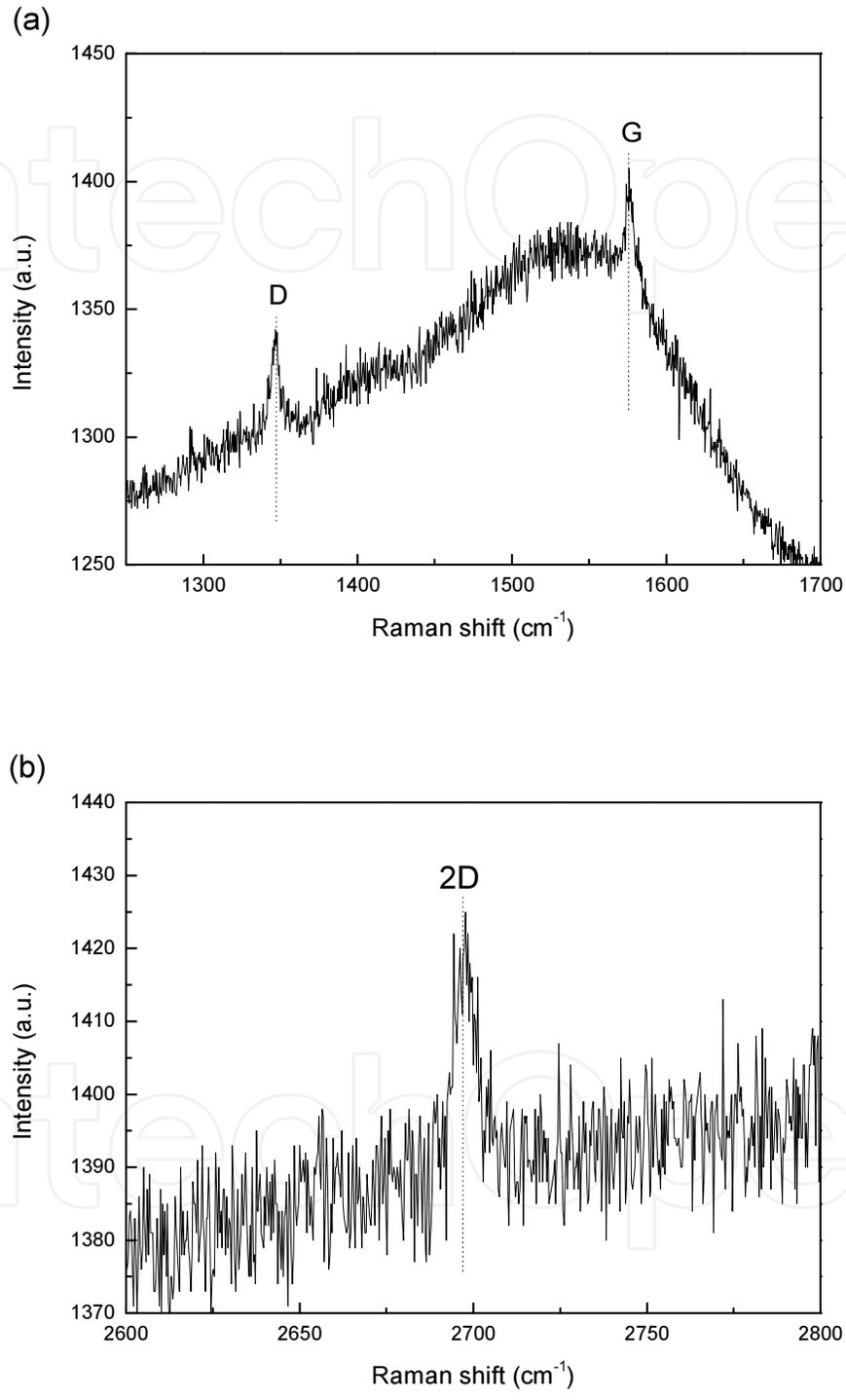

Figure 13. Raman scattering spectra of graphene film deposited on glass substrate. The spectra include important peaks that correspond to the D-band (1,350 cm^{-1}), the G-band (1,580 cm^{-1}), and the 2D-band (2,700 cm^{-1}) [17]

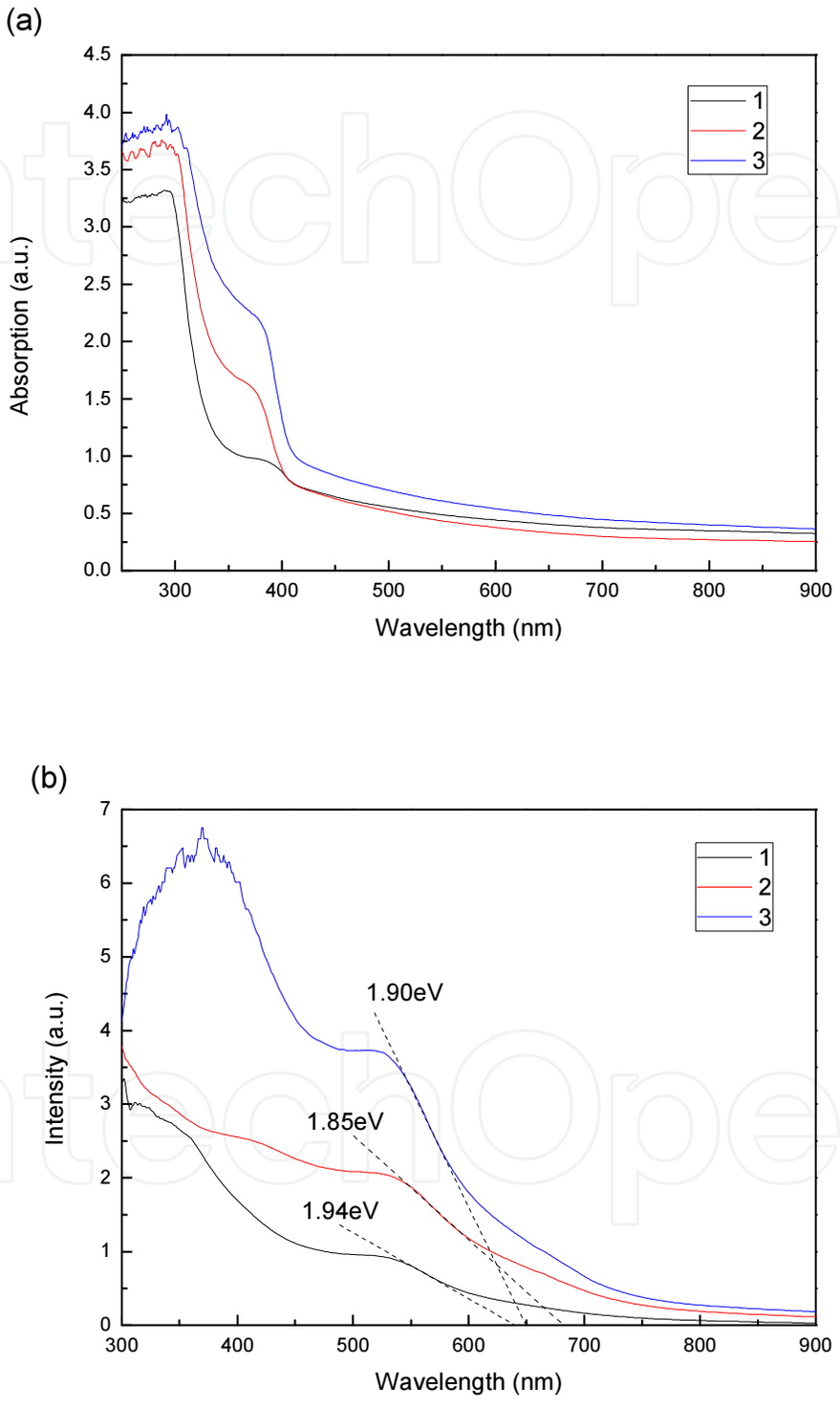

Figure 14. UV-vis absorption spectra of DSSCs with different structures (a) before and (b) after dye loading [17]

http://dx.doi.org/10.5772/60644

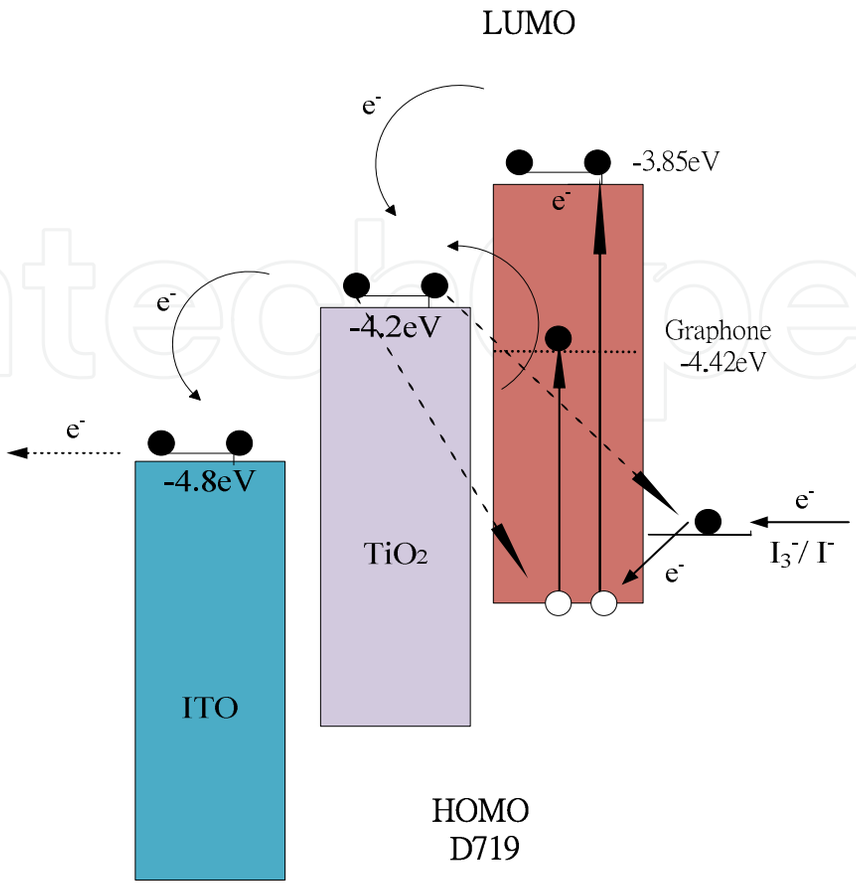

Figure 15. Energy level diagram and mechanism of photocurrent generation in DSSCs with TiO_2 /graphene/TiO_2 sandwich structure [17]

6. Conclusion

To enhance the performance of DSSCs, this work used nanostructure graphene electron transfer layer by plating or sputtering and compared the difference between the DSSC structure with graphene/TiO_2 and with TiO_2/graphene/TiO_2. From the I-V curves, sputtered graphene is much better than plated graphene because the plated graphene has a scattered distribution of ITO. The enhanced performance of DSSCs with a graphene may be attributed to the increase in electron transport efficiency and light absorption in visible range, especially in the range of 310–400 nm. Therefore, the efficiency of conversion of solar energy with graphene+TiO_2 to electricity were increased from 1.45 % to 3.98 %, and the efficiency of conversion of solar energy with TiO_2/graphene/TiO_2 sandwich structure to electricity was increased from 1.38 % to 3.93 %, respectively, under simulated full-sun illumination. This improvement in performance is associated with an increase in the absorption of light, a wide range of absorption wavelengths, shorter charge transportation distances, and the suppression of charge recombination when the graphene is applied.

Author details

Lung-Chien Chen

Address all correspondence to: ocean@ntut.edu.tw

Department of Electro-optical Engineering, National Taipei University of Technology, Taipei, Taiwan

References

[1] T. Bora, H. H. Kyaw, S. Sarkar, S. K. Pal, and J. Dutta, "Highly efficient ZnO/Au Schottky barrier dye-sensitized solar cells: role of gold nanoparticles on the charge-transfer process," Beilstein J Nanotech, vol. 2, no. 1, 681–690, 2011.

[2] C. Hagglund, M. Zach, and B. Kasemo, "Enhanced charge carrier generation in dye sensitized solar cells by nanoparticle plasmons," Appl. Phys. Lett., vol. 92, no. 1, 2008.

[3] S. Barazzouk and S. Hotchandani, "Enhanced charge separation in chlorophyll a solar cell by gold nanoparticles," J. Appl. Phys., vol. 96, no. 12, 7744–7746, 2004.

[4] S. W. Tong, C. F. Zhang, C. Y. Jiang et al., "Improvement in the hole collection of polymer solar cells by utilizing gold nanoparticle buffer layer," Chem. Phys. Lett., vol. 453, no. 1–3, 73–76, 2008.

[5] L. C. Chen, C. C. Wang, and B. S. Tseng, "Enhancement in nano-crystalline TiO2 solar cells sensitized with ZnPc by nanoparticles, " J Optoelectron Biome.,vol.1, no.3, 249–254, 2009.

[6] X. Du, I. Skachko, A. Barker, and E. Y. Andrei, "Approaching ballistic transport in suspended grapheme," Nat Nanotechnol., vol. 3, no. 8, 491–495, 2008.

[7] R. R. Nair, P. Blake, A. N. Grigorenko et al., "Fine structure constant defines visual transparency of graphene," Science, vol. 320, no. 5881, 1308, 2008.

[8] X. Wang, L. Zhi, N. Tsao, Z. Tomovic, J. Li, and K. M. Mullen, "Transparent carbon films as electrodes in organic solar cells," Angew Chem. Int. Edit., vol. 47, no. 16, 2990–2992, 2008.

[9] X. Wang, L. Zhi, and K. Mullen, "Transparent, conductive graphene electrodes for dye-sensitized solar cells," Nano Lett., vol. 8, no. 1, 323–327, 2008.

[10] S. Bae, H. Kim, Y. Lee et al., "Roll-to-roll production of 30-inch graphene films for transparent electrodes," Nat. Nanotechnol, vol. 5, no. 8, 574–578, 2010.

[11] D. W. Chang, H. J. Choi, A. Filer, and J. B. Baek, "Graphene in photovoltaic applications: Organic photovoltaic cells (OPVs) and dye-sensitized solar cells (DSSCs)", J. Mater. Chem. A, vol. 2,12136–12149, 2014.

[12] C. H. Hsu, J. R. Wu, L. C. Chen, P. S. Chan, and C. C. Chen, "Enhanced performance of dye-sensitized solar cells with nanostructure graphene electron transfer layer," Adv. Mater. Sci. Eng, 107352, 2014.

[13] H. Zhang, W. Wang, H. Liu, R. Wang, Y. Chen, and Z. Wang, "Effects of TiO2 film thickness on photovoltaic properties of dye-sensitized solar cell and its enhanced performance by graphene combination," Mater. Res. Bull., vol. 49, 126–131, 2014.

[14] H. N. Kim, H. Yoo, and J. H. Moon, "Graphene-embedded 3D TiO2 inverse opal electrodes for highly efficient dye-sensitized solar cells: Morphological characteristics and photocurrent enhancement," Nanoscale, vol. 5, 4200–4204, 2013.

[15] C. Yang, H. Bi, D. Wan, F. Huang, X. Xie, and M. Jiang, "Direct PECVD growth of vertically erected graphene walls on dielectric substrates as excellent multifunctional electrodes," J. Mater. Chem. A, vol. 1, 770–775, 2013.

[16] B. Tang and G. Hu, "Two kinds of graphene-based composites for photoanode applying in dye-sensitized solar cell," J. Power Source, vol. 220,95–102, 2012.

[17] L. C. Chen, C. H, Hsu, P. S. Chan, X. Zhang, and C. J. Huang, "Improving the performance of dye-sensitized solar cells with TiO2/graphene/TiO2 sandwich structure," Nanoscale Res. Lett., vol. 9, 380, 2014.

[18] M. Koshino and T. Ando, "Electronic structures and optical absorption of multilayer graphenes," Solid State Commun., vol. 149, no. 27-28, 1123–1127, 2009.

[19] G. Giovannetti, P. A. Khomyakov, G. Brocks, V. M. Karpan, J. van den Brink, and P. J. Kelly, "Doping graphene with metal contacts," Phys. Rev. Lett., vol. 101, no. 2, 2008.

[20] R. Czerw, B. Foley, D. Tekleab, A. Rubio, P. M. Ajayan, and D. L. Carroll, "Substrate-interface interactions between carbon nanotubes and the supporting substrate," Phys. Rev. Lett. B, vol. 66, 2002.

[21] A. Kongkanand, R. Martinez-Dominguez, and P. V. Kamat, "Single wall carbon nanotube scaffolds for photoelectron chemical solar cells. Capture and transport of photogenerated electrons," Nano. Lett., vol. 7, no. 3, 676–680, 2007.

[22] F. Xu, J. Chen, and X. Wuetal, "Graphene scaffolds enhanced photogenerated electron transport in ZnO photoanodes for high- efficiency dye-sensitized solar cells," J Phys. Chem. C, vol. 117, 8619–8627, 2013.

[23] A. C. Ferrari, J. C. Meyer, V. Scardaci, C. Casiraghi, M Lazzeri, F. Mauri, S. Piscanec, D. Jiang, K. S. Novoselov, S. Roth, and A. K. Geim, "Raman spectrum of graphene and graphene layers," Phys. Rev. Lett., vol. 97, 187401, 2006.

[24] X. L. Fang, M. Y. Li, K. M. Guo, Y. D. Zhu, Z. Q. Hu, X. L. Liu, B. L. Chen, and X. Z. Zhao, "Photoelectrodes modification by N doping for dye-sensitized solar cells," Electrochim. Acta 65, 174–178, 2012.

[25] X. L. Fang, M. Y. Li, K. M. Guo, X. L. Liu, Y. Zhu, B. Sebo, and X. H. Zhao, "Graphene-compositing optimization of the properties of dye-sensitized solar cells Solar," Energy, vol. 101, 176–181, March 2014.

[26] Y. Y. Wang, Z. H. Ni, T. Yu, Z. X. Shen, H. M. Wang, Y. H. Wu, W. Chen, and A. T. S. Wee, "Raman studies of monolayer graphene," The Substrate Effect J. Phys. Chem. C, vol. 112, no. 29, 10637–10640, 2008.

[27] J. N. Zheng, S. S. Li, F. Y. Chen, N. Bao, A. J. Wang, J. R. Hen, and J. J. Feng, "Facile synthesis of platinum–ruthenium nanodendrites supported on reduced graphene oxide with enhanced electrocatalytic properties," J Power Sources, vol. 266, 259–267, 2014.

[28] AZoM, "Characterization of graphene using Raman spectroscopy," http://www.azom.com/article.aspx?ArticleID=6271.

[29] M. Huang, H. Yan, T. F. Heinz, and J. Hone, "Probing strain-induced electronic structure change in graphene by Raman spectroscopy," Nano Lett., vol. 10, 4074–4079, 2010.

[30] O. Frank, M. Mohr, J. Maultzsch, C. Thomsen, I. Riaz, R. Jalil et al. "Raman 2D-band splitting in graphene," Theory Expt ACS Nano., vol. 5, no. 3, 2231–2239, 2011.

[31] D. Yoon, Y. W. Son, and H. Cheong, "Strain-dependent splitting of the double-resonance Raman scattering band in graphene," Phys. Rev. Lett., vol. 106, no. 15, 155502-1–4, 2011.